CORE
Metadata, citation and similar papers at core.ac.uk
Provided by Warwick Research Archives Portal Repository

Manuscript version: Author's Accepted Manuscript
The version presented in WRAP is the author's accepted manuscript and may differ from the published version or Version of Record.

Persistent WRAP URL:
http://wrap.warwick.ac.uk/111011

How to cite:
Please refer to published version for the most recent bibliographic citation information. If a published version is known of, the repository item page linked to above, will contain details on accessing it.

Copyright and reuse:
The Warwick Research Archive Portal (WRAP) makes this work by researchers of the University of Warwick available open access under the following conditions.

Copyright © and all moral rights to the version of the paper presented here belong to the individual author(s) and/or other copyright owners. To the extent reasonable and practicable the material made available in WRAP has been checked for eligibility before being made available.

Copies of full items can be used for personal research or study, educational, or not-for-profit purposes without prior permission or charge. Provided that the authors, title and full bibliographic details are credited, a hyperlink and/or URL is given for the original metadata page and the content is not changed in any way.

Publisher's statement:
Please refer to the repository item page, publisher's statement section, for further information.

For more information, please contact the WRAP Team at: wrap@warwick.ac.uk.

warwick.ac.uk/lib-publications

Polar Domain Structural Evolution under Electric Field and Temperature in the $(Bi_{0.5}Na_{0.5})TiO_3$-0.06$BaTiO_3$ Piezoceramics

Jinyan Zhao,[a, b] *Nan Zhang,*[a, *] *Wei Ren,*[a, *] *Gang Niu,*[a] *David Walker,*[c] *Pamela A. Thomas,*[c] *Lingyan Wang,*[a] *and Zuo-Guang Ye*[b, a, *]

[a]Electronic Materials Research Laboratory, Key Laboratory of the Ministry of Education & International Center for Dielectric Research, School of Electronic and Information Engineering, Xi'an Jiaotong University, Xi'an 710049, China

[b]Department of Chemistry and 4D LABS, Simon Fraser University, Burnaby, British Columbia, V5A 1S6, Canada.

[c]Department of Physics, University of Warwick, Coventry CV4 7AL, United Kingdom.

[*]Corresponding authors: wren@mail.xjtu.edu.cn; nzhang1@mail.xjtu.edu.cn; zye@sfu.ca.

Abstract

Lead-free bismuth sodium titanate and related compounds are of great interest as promising candidates for piezoelectric applications. However, the full understanding of this family of materials is still a challenge partly because of their structural complexity and different behaviors with or without the application of an external electric field. Here, piezoresponse force microscopy is used to gain insight into the mesoscopic-scale domain structure of the morphotropic phase boundary (MPB) composition of (1-x)$Bi_{0.5}Na_{0.5}TiO_3$-$x$$BaTiO_3$ solid solution at x = 0.06 (abbreviated as BNT-6BT). The evolution of the domains with the changes of the electric field and temperature has been thoroughly examined in conjunction with the crystal structure analysis and dielectric studies. It is

found that ferroelectric domains with size of hundreds of nanometers are embedded in a relaxor state without visible domains on a mesoscopic scale, which are considered to contribute to the tetragonal and cubic phases in the material, respectively. Temperature-independent domain configuration is observed in the unpoled sample from room temperature to 200 ^{o}C. While, temperature-dependent domain configuration is observed in the poled sample. The homogenously poled state breaks into the mixed domain configuration containing polydomain structure and invisible state around the so-called depoling temperature. The structural changes on different length scales are also discussed. This work provides an in-depth understanding of the structural and domain changes under an electric field and the temperature-dependent domain evolution in both unpoled and poled states in the BNT-BT solid solution of the MPB composition.

1. Introduction

As one of the promising lead-free candidates for replacing the lead-containing ferroelectric compounds, the (1-*x*)$Bi_{0.5}Na_{0.5}TiO_3$-*x*$BaTiO_3$ (abbreviated as BNT-100*x*BT) solid solution has been extensively studied for potential applications in high-frequency ultrasonic transducers and piezoelectric actuators, due to its excellent dielectric and piezoelectric properties [1-3]. Although the compositions of the morphotropic phase boundary (MPB) in this system were reported to range from x = 0.05 to x = 0.11 based on the structural analysis by X-ray diffraction and Raman spectroscopy [4-7], the enhanced dielectric, ferroelectric and piezoelectric properties appear only in the composition range of x = 0.06 - 0.07 [6, 8], which is commonly believed to be the true MPB with the coexistence of a rhombohedral and a tetragonal ferroelectric phase [9]. The MPB separates a rhombohedral or monoclinic symmetry (*R*3*c* or *Cc*) in the BNT-rich composition and a tetragonal

symmetry (*P*4*mm*) in the BT-rich composition [1]. However, compared with other ferroelectric perovskites, BNT-BT exhibits a very small structural distortion from its parent cubic phase, which makes it difficult to directly distinguish the different phases using conventional diffraction techniques [10-12]. Therefore, the average and local structures of this solid solution, especially near the MPB, are still under extensive debate. Recently, several studies speculated that the MPB of BNT-BT has a cubic-like structure, and the application of an electric field induces a phase transition from a cubic-like to the tetragonal phase or a mixture of different structures, resulting in enhanced piezoelectric properties [13, 14]. Groszewicz *et al*. [15] reported the coexistence of a cubic phase and a polar state in BNT-6BT on the atomistic scale by means of quadrupolar ^{23}Na nuclear magnetic resonance (NMR). The cubic phase existing in the unpoled sample vanishes under the application of a high electric field, and recovers upon thermal annealing and zero-electric-field cooling process.

Besides the uncertainty on its average and local crystal structures, studies on the mesoscopic-scale domain configuration and the electric field-induced domain structural changes are also lacking. The dielectric and piezoelectric properties in ferroelectric materials are generally dependent on both intrinsic and extrinsic mechanisms. Intrinsic contributions are the collective deformation originating from individual unit cells' distortions, regardless of the domain structure. Extrinsic contributions mainly arise from the domain wall motion. Therefore, the domain wall mobility and density are responsible for the extrinsic dielectric and piezoelectric properties of ferroelectric materials [16-18].

In this work, the domain evolutions under electric field and temperature change in the MPB composition (BNT-6BT) are systematically investigated in relation to the dielectric response and crystal structure. It should be noted that the MPB compositions reported in the literatures vary due to the different ceramics preparation processes and testing methods. Therefore, compositions with *x*

from 0 to 0.08 are prepared in this work and the MPB composition is determined to be at x = 0.06 (BNT-6BT) with the highest permittivity and piezoelectric coefficient. The domain-related study is performed by the piezoresponse force microscopy (PFM) [19, 20], in which a high spatial resolution is achieved by using a sharp conductive tip, offering a non-destructive way to study both the out-of-plane and in-plane domain structures in polycrystalline materials at various temperatures. We aim to investigate the behavior of BNT-BT under electric field from a multi-scale approach, and to provide better understanding in the mechanism of the electrical properties in BNT-BT solid solutions at the MPB in relation to its complex morphotropic structure.

2. Experimental Procedure

Ceramic samples were prepared using solid-state synthesis from reagent-grade Bi_2O_3, TiO_2, Na_2CO_3 and $BaCO_3$ according to the stoichiometric composition of BNT-6BT. The reactant powders were firstly mixed and calcined at 900 ^oC for 2 hours. After calcination, the ground and ball-milled powder was densified into pellets at 120 MPa, and then sintered at 1150 ^oC for 2 hours. The average density of 5.817 g/cm^3 of the sintered pellets was determined by the Archimedes drainage method. The sintered pellets were polished and coated with silver paste for electrical measurements. The dielectric response was measured using the broadband dielectric spectrometer (Novocontrol GmbH, Germany). For X-ray diffraction (XRD) measurements, the sintered ceramics were smashed and milled into fine powder, which was then annealed to remove the mechanical stress. High-resolution X-ray powder diffraction experiments were performed on a P'Analytical X'pert Pro diffractometer with a curved Johansson monochromator, providing focused Cu Kα1 radiation. For the piezoresponse force microscopy (PFM) measurements, the sintered pellets were mirror-polished

using aluminium oxide paper with coated abrasive particle sizes of 9 µm, 5µm, 3µm, and 1µm. The domain structure was investigated using the PFM mode of a scanning probe microscopy (Dimension Icon, Bruker, USA) equipped with a heating stage. The measurements were performed using a conductive tip (resonant frequency at 40 kHz, DDESP, Bruker). An ac voltage (15 ~ 45 kHz, 6 V) was applied on the sample stage to stimulate the sample expansion and shrink and the conductive tip was used as the top electrode.

3. Results

Fig. 1(a) shows the dielectric response (real and imaginary part of the permittivity) in an unpoled sample. The relaxor behavior is observed in the unpoled sample, as evidenced by the temperature and frequency dependences of permittivity, which is in agreement with previous reports [11, 21]. There are two anomalies observed in the temperature-dependent dielectric response (the real part, ε′). One of them is a broad and frequency- and temperature-dependent dielectric shoulder around T_s [22] between 90 ^oC and 150 ^oC, and the other is a broad permittivity maximum at around 300 ^oC, which is sometimes determined as T_{max} [2]. However, in our study, we find that the permittivity at higher temperature is not frequency dependent [7, 23, 24]. On the other hand, the lower-temperature broad anomaly (T_s) is more likely to be related to the relaxor behavior of this system [2, 7, 11, 22, 25, 26], which will be discussed in detail later. The frequency dispersion of the real part (ε′) appears from below room temperature to 150 ^oC and vanishes above that point. The frequency-dependent permittivity values measured at various temperatures shown in Fig. 1(b) also confirm this tendency. The temperature-dependent imaginary part (ε″) in Fig. 1(a) exhibits considerable dielectric relaxation around T_s. The temperature of the dielectric loss (imaginary part) maximum peak increases with

increasing frequency, confirming that the ceramics exhibits relaxor ferroelectricity.

The dielectric response of the poled sample is strikingly different from that in the unpoled sample, as shown in Fig. 1(c). Before poling, the frequency dispersion appears at room temperature; after poling, the frequency dispersion in the ε′ and ε″ is significantly attenuated at room temperature, meaning that the electric field has induced the transition from the relaxor state to a macroscopic ferroelectric state, in agreement with the high-energy X-ray diffraction results that an electric field induced a structure transition from the cubic to a lower symmetry phase [13, 27]. An abnormal of ε″ at high frequency is due to the big loss after poling. Upon heating, the poled sample shows a sharp increase in dielectric constant around $T_d \approx 76$ °C, above which the frequency dispersion recurs, as in the unpoled sample, indicating a transformation from the induced ferroelectric state back to the relaxor state as in the case of the conventional relaxor PMN [25]. It is also observed in Fig. 1(d) that a resonance peak (which is a demonstration of the poled state in piezoelectric ceramic) appears at high frequency below 74 °C and vanishes above 78 °C. Therefore, $T_d = 76$ °C is determined as the depoling temperature (T_d) in this case. This result is in good agreement with the reported depoling temperature (73-75 °C) measured from the thermally induced depolarization current [28]. In order to quantitatively analyze the frequency dispersion, the slopes of ε′ versus log-frequency whose absolute value is positively corrected with the dispersion degree at various temperatures were calculated in both unpoled (S_u) and poled (S_p) samples and the results are shown in Fig. 1(e), together with the ratio of S_u/S_p. The degree of frequency dispersion reaches its maximum at T_d in the unpoled BNT-6BT ceramic as the absolute value of the slope peaks. The absolute value of the slope in the poled BNT-6BT is approximately close to zero at room temperature with a rapid change around T_d, and then follows the track of the unpoled sample above T_d with further increase of temperature. When the temperature increases above

T_s, the frequency dispersion vanishes completely in both unpoled and poled ceramics with a flat slope approaching zero.

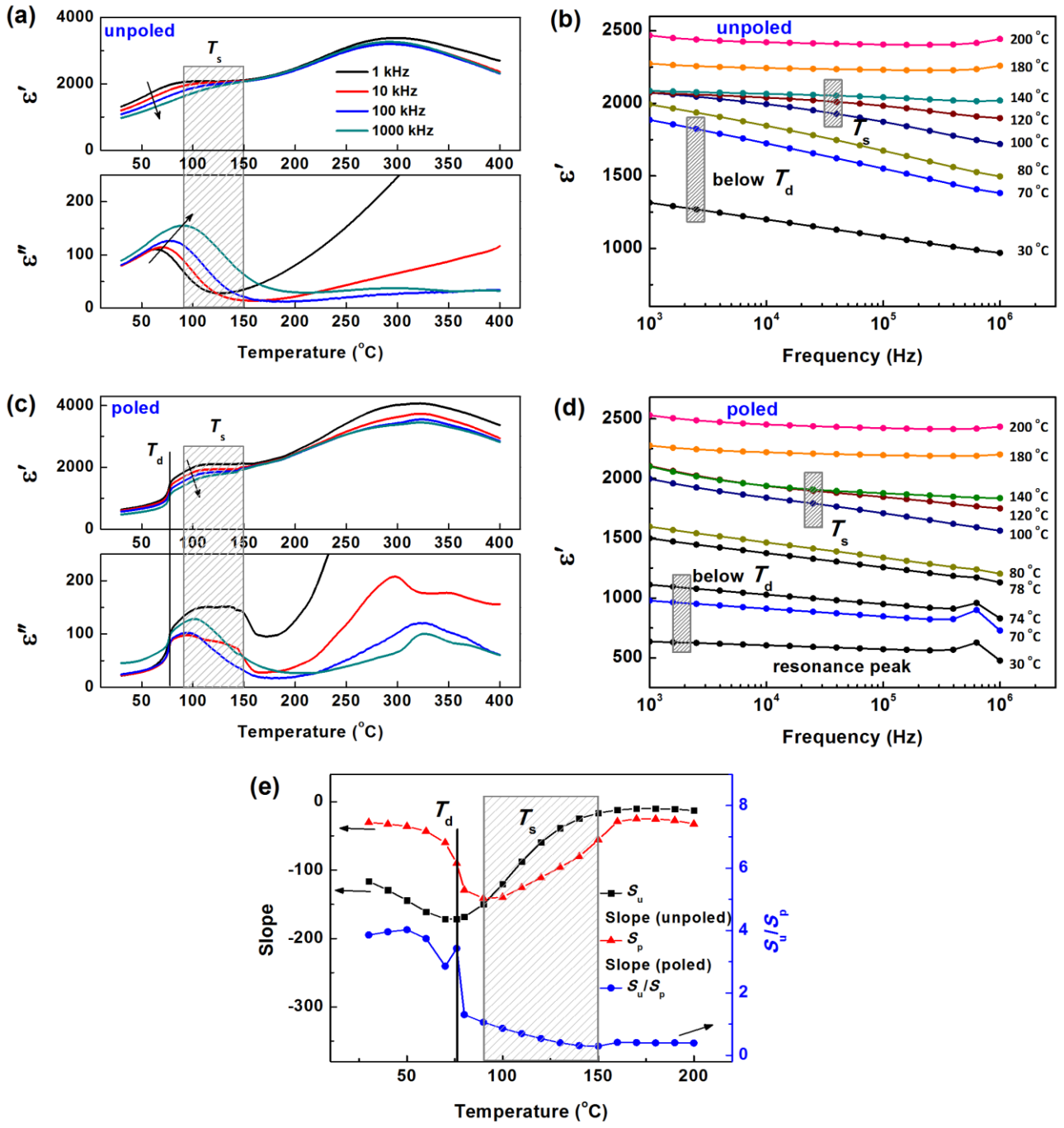

Fig. 1 The real part of permittivity (ε′) and imaginary part of permittivity (ε″) of the BNT-6BT ceramics measured at various frequencies and temperatures. (a) ε′ and ε″ plotted versus temperature at various frequencies for unpoled sample. (b) ε′ plotted versus log-frequency at various temperatures

for unpoled sample. (c) ε′ and ε″ plotted versus temperature at various frequencies for poled sample. (d) ε′ plotted versus log-frequency at various temperatures for poled sample. (e) The slope of ε′ versus log-frequency as a function of temperature for both unpoled sample (S_u) and poled sample (S_p), as well as the ratio of S_u/S_p.

The crystal structure of the BNT-6BT powder was investigated by high-resolution X-ray powder diffraction experiments. The structural models were obtained by Rietveld refinement using the software TOPAS-Academic (Alan Coelho, http://www.topas-academic.net/). The diffraction pattern was firstly refined with a cubic structure of models due to the fact that the frequency dependences of the dielectric response suggest a relaxor behavior, which mostly exists in a long-range cubic phase with a coexistence of rhombohedral and tetragonal domains at the local scale [25]. However, because of the asymmetrical shape of many Bragg peaks in the diffraction pattern, a single cubic (*Pm*-3*m*) structural model cannot fit the data well. Considering that the shoulders of the {200} Bragg reflection underneath the sharp main peak in the middle may be arises from the split of the tetragonal (200)/(020) and (002) peaks, a tetragonal phase (*P4mm*) component is taken into account to refine the XRD results. In addition, the rhombohedral phase (*R*3*c*) was reported to exist in the MPB composition [29-31]. We note that in some cases, the asymmetrical line broadening in the powder diffraction patterns is caused by anisotropic micro-strains [32] and can be refined in the Rietveld refinement. However, incorporating the anisotropic micro-strain line broadening parameters in our refinements did not improve the result. Therefore, two models of mixed phases: rhombohedral + tetragonal (T+R), and tetragonal + cubic (T+C), and the single-phase cubic (C) model were tested. Fig. 2(a) shows the XRD patterns in a limited 2θ range of the BNT-6BT powder measured at 25 ^{o}C

and the refined patterns. There are several regions in the diffraction pattern showing remarkable difference between the experimental data and refinement curve using C and T+R models. For example, the refinement curve almost coincide with the experimental data of the {200} Bragg reflection using the T+C model, while, neither the shoulders nor the main peak can be fitted well using the C and T+R models. Peak splits can also be observed in the {211} Bragg reflection. C and T+R models fail to fit the lower peak on the left side. The refined parameters using the three kinds of modes are shown in Table 1. The T+C model gives the best fit for the whole pattern on the peak position, peak width, and peak height, as shown in Fig. 2(b). This refinement result suggests the coexistence of a tetragonal and a cubic phases in the BNT-6BT ceramics. It is believed that the cubic phase is non-centrosymmetric at the local scale, possibly with the coexistence of R and/or T distortions.

To study the phase transformation around T_d, the structural evolution as a function of temperature measured upon heating are analyzed. No obvious phase transition is observed from room temperature to 250 ^oC, as shown in the 2θ contour plot around the {200} Bragg reflection (Fig. 2(b)). At room temperature, the shoulders are attributed to the (002) and (200)/(020) peaks of the tetragonal phase, and the middle (200) peak belongs to the cubic phase. Upon heating, the {200} peaks shift to lower angles, while the shape is still maintained with the shoulders subsisting up to 250 ^oC, the highest measurement temperature. As expected, the XRD results measured at 250 ^oC are also refined well with the model of T+C phases. Raman spectroscopic measurement also confirmed that the structure of the MPB composition above 100 ^oC is identical to that below 100 ^oC [7]. Similarly, the dielectric anomaly around T_s was also observed in pure BNT below the temperature where the permittivity maximum appears, and no phase transition was evidenced going through the T_s [33-35]. The

intensity of the {200} Bragg reflection peak increases at higher temperature. This is an indication of the decreasing full width at half maximum (FWHM), which may be related to the decrease in disorder of the cubic component. The combined X-ray powder diffraction and dielectric permittivity results suggest that the T_s observed in our BNT-6BT ceramic most likely corresponds to the relaxor behavior arising from a slowing down of the dynamics of polar nanoregions in the cubic phase, rather than a long-range ferroelectric-paraelectric phase transition in the tetragonal component. This tetragonal component must exist in the local scale and it persists (and possibly remains unchanged) up to at least 250 ^{o}C.

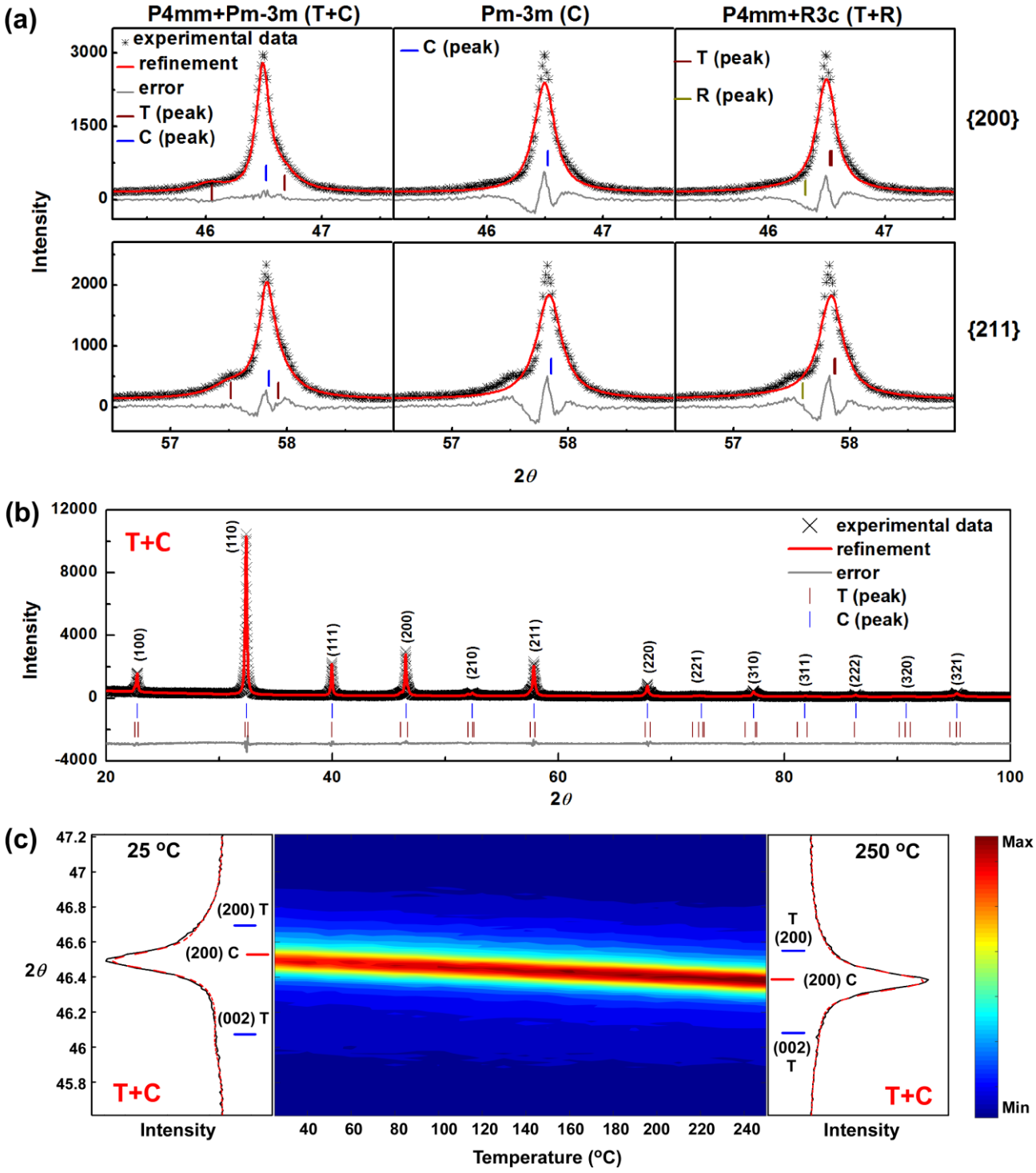

Fig. 2 Structural analysis of the BNT-6BT ceramic powder by Rietveld refinement. (a) The experimental data, refinement and error plots of {200} and {211} Bragg profiles after Rietveld refinement with the structural models of T+C, C and T+R. The dark red, blue and dark yellow vertical bars correspond to the peak positions of T, C and R phases, respectively. (b) XRD patterns of

the ceramic powder measured at 25 ^{o}C and the refinement plot with the model of T+C. The blue and red vertical bars correspond to the peak positions of T and C phases, respectively. (c) Mapping of {200} Bragg profile as a function of temperature, accompanied with the refinements of {200} Bragg profile measured at 25 ^{o}C and 250 ^{o}C with the model of T+C on both sides of the 2D picture.

Table 1 Refined structural parameters and atomic positions of the BNT-6BT ceramic powder using models of T+C, C and T+R.

T+C model			**T phase**			**C phase**	
a, *b*, *c* (Å)		3.8874(2)	3.8874(2)	3.9386(5)	3.9003(1)	3.9003(1)	3.9003(1)
Na/Bi/Ba	x, y, z	0	0	0.01(3)	0	0	0
Ti	x, y, z	0.5	0.5	0.58(3)	0.5	0.5	0.5
O1	x, y, z	0.5	0.5	0	0.5	0.5	0
O2	x, y, z	0	0.5	0.5			
R_{bragg}	Phase fraction	2.76	31%		2.03	68%	
C model							
a, *b*, *c* (Å)		3.9001(1)	3.9001(1)	3.9001(1)			
Na/Bi/Ba	x, y, z	0	0	0			
Ti		0.5	0.5	0.5			
O1		0.5	0.5	0			
R_{bragg}	Phase fraction	2.47	100%				
T+R model			**T phase**			**R phase**	
a, *b*, *c* (Å)		3.899(2)	3.899(2)	3.900(1)	5.532(2)	5.532(2)	13.54(2)
Na/Bi/Ba	x, y, z	0	0	0.01(4)	0	0	0.27(2)
Ti	x, y, z	0.5	0.5	0.49(6)	0	0	-0.01(2)
O1	x, y, z	0.5	0.5	0	0.09(2)	0.19(4)	0.0833
O2	x, y, z	0	0.5	0.5			
R_{bragg}	Phase fraction	2.44	84%		2.33	16%	

To further investigate the structural evolution under an electric field, we have studied the mesoscopic domain structures in both unpoled and poled BNT-6BT ceramics using PFM. Poling was performed

at room temperature under 4.5 kV/cm for 15 minutes, and a d_{33} value of 144 pC/N was obtained in the poled sample. Fig. 3(a) depicts the domain structure of the unpoled BNT-6BT sample. Two kinds of PFM responses are observed in both the out-of-plane and in-plane images. One is the areas shown by clear domain patterns with a strong amplitude response (encircled by dark lines), and the other is the surrounding areas containing domains with a weak amplitude response and a blurry phase, *i.e.*, nanodomains "invisible" to PFM. This is similar to the nanodomains observed by TEM on microscopic scale in the MPB composition [31]. The application of the electric field increases the domain size in the whole measured region as shown in the dramatically different out-of-plane and in-plane images observed in poled sample in Fig. 3(b). The out-of-plane phase component shows that the whole measured area is switched almost completely with the polarization pointing in the upward direction. The corresponding amplitude component exhibits strong response in the whole poled area. Because the polycrystalline ceramics are randomly oriented, the in-plane phase component exhibits a random distribution of polarization, including regions with in-plane component pointing towards left (labeled as A), regions with in-plane component pointing towards right (labeled as B) and also regions with blurry phase contrast (labeled as C). Correspondingly, the in-plane amplitude component exhibits strong response in region A and B, and no response in region C. Fig. 3(c) describes the schematic of the polarization distribution of the poled BNT-6BT ceramic. Suppose that the out-of-plane phase exhibits a response perpendicular to the surface (*z* axis) and the in-plane phase shows a response parallel to the surface (*x* axis). Both the out-of-plane and in-plane phases constitute the polarization orientation state in the *x*-*z* projection, with a left oblique polarization in region A, a right oblique polarization in region B, and an upwards polarization in region C, depending on the orientation of the grains. Fig. 3(d) shows the schematic of the domain structure and polarization

status before and after poling when view on perpendicular to the *x*-*z* plane. Before poling, the ceramic exhibits randomly orientated domains and 180° domain walls in a single grain. After poling, the domains are switched towards the orientations formed by the electric field and 180° domain walls inside of single grain are diminished.

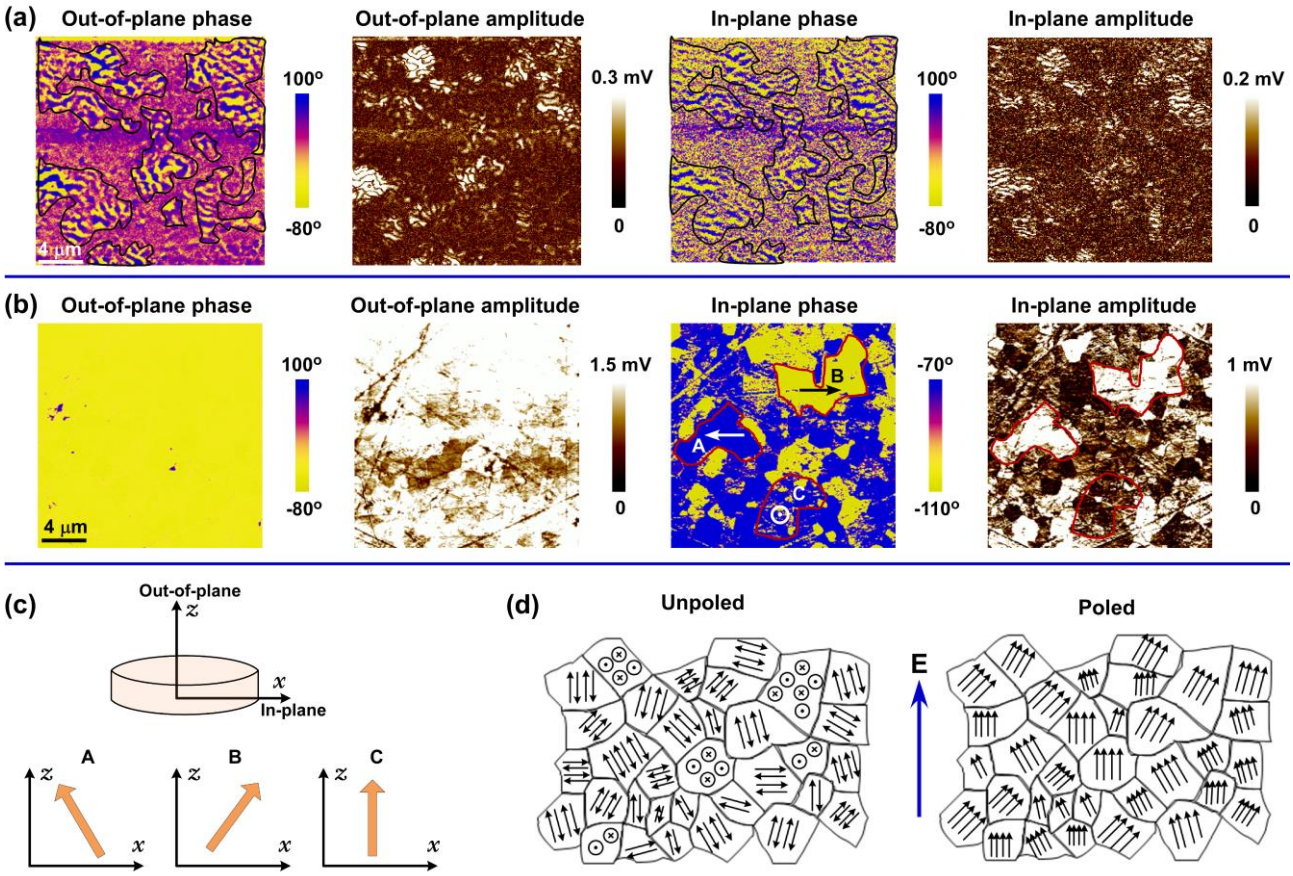

Fig. 3 PFM images of the unpoled (a) and poled (b) BNT-6BT ceramics, including the out-of-plane phase and amplitude images, in-plane phase and amplitude images. (c) Schematic of the polarization orientation in a poled BNT-6BT ceramic marked in (b). (d) Schematic of the domain structure and polarization orientation in polycrystalline ceramics before and after poling.

In order to further understand the evolution of the polar state, the temperature-dependent domain

structures in both unpoled and poled samples are investigated. The stability of the polar domain and polarization responses as a function of temperature in the unpoled BNT-6BT sample are demonstrated in Fig. 4. Our analysis is focused on one of the areas that already show clear domain patterns before poling. Distinct phase contrast and strong amplitude response are present in the PFM images from 50 ^{o}C to 120 ^{o}C. With temperature increasing to 200 ^{o}C, the amplitude response drops and the phase contrast becomes blurred. Upon cooling down to room temperature, both the intense amplitude response and the distinct phase contrast recover. No variation in the domain patterns is observed from room temperature up to 200 ^{o}C, *i.e.*, going through T_d and T_s. Similarly, it was reported that the domain structure does not change going through the T_s in BNT single crystals [36, 37]. Fig. 4(i) provides the relative changes of piezoresponse signal of the scanned area as a function of temperature for the BNT-6BT sample measured upon heating. The average PFM amplitude signals from room temperature to 250 ^{o}C were fitted using a linear function. With increasing temperature, the polarization response gradually weakenes, possibly due to the thermally weakened ferroelectricity. More interestingly, the piezoelectric response does not vanish completely, as seen from both the PFM image and the signal strength plot at or above 200 ^{o}C. If the polarization observed in this domain corresponds to the tetragonal component in X-ray diffraction, the temperature evolution of this phase fits well the XRD result that a complete paraelectric phase does not show up in the experimental temperature range. This temperature-dependent mesoscopic scale polarization response is also in agreement with the macroscopic scale polarization response based on the polarization hysteresis loops reported by Jo *et al.*, which seemed to suggest that there is still a nonzero remanent polarization at 230 ^{o}C [38].

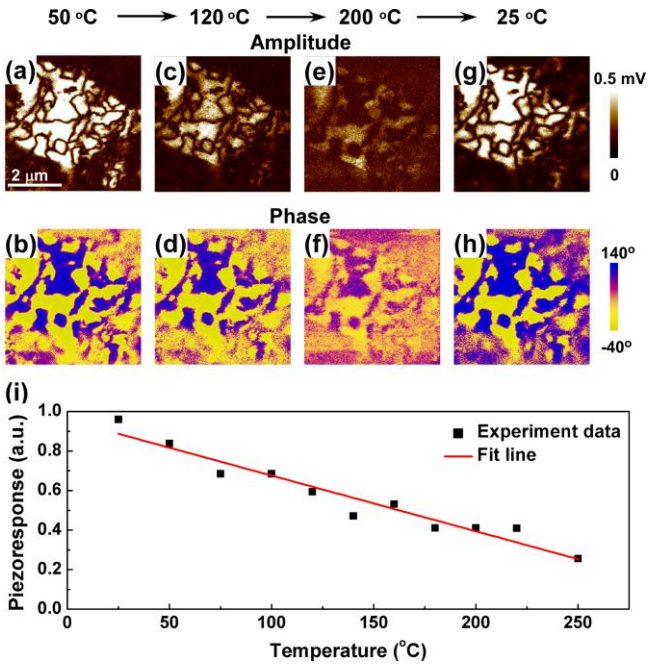

Fig. 4 Temperature-dependent piezoresponse evolution in an unpoled BNT-6BT ceramic. Out-of-plane amplitude images at various temperature: (a) 50 °C, (c) 120 °C, (e) 200 °C, and (g) 20 °C, respectively. Out-of-plane phase images at various temperature, (b) 50 °C, (d) 120 °C, (f) 200 °C, and (h) 20 °C, respectively. (i) The relative change of piezoresponse as a function of heating temperature and the linear fitting result.

A positive DC voltage of 40 V was applied to the tip during scanning to pole domains inside the inner square, then the poled domain state was examined upon heating. The analysis was focused on the whole poled region containing distinct domain patterns that constrast the "invisible" domain features before poling. The evolution of the out-of-plane PFM amplitude and phase images after poling as a function of temperature is presented in Fig. 5. As shown in Fig. 5(a-b), there are two types of regions in the poled area, *i.e.*, the area originally occupied by domains with a strong amplitude response and distinct phase before poling (labeled as A), and the surrounding area containing domains with a weak amplitude response and blurry phase before poling (labeled as B).

At room temperature, external electrical field induces a long-range ordered polarization, as shown in Fig. 5(c-d). During the poling process, random domains are switched to one preferred orientation in region A, while the long-range ordered polarization is developed in region B. The mesoscopic polarization response unvaries up to 50 ^{o}C. With further increase of temperature, the PFM response in the poled region B vanishes below 90 ^{o}C (higher than the T_d), while the mesoscopic polarization in the poled region A returns to randomly oriented polarizations with a weaker response. With temperature increasing to 150 ^{o}C, a weak PFM response subsists in region A, similar to the phenomenon described in Fig 4. Upon cooling to 75 ^{o}C, the PFM response looks similar to that at 90 ^{o}C, *i.e.* with no domain-related features in region B and a random polarization distribution in region A, indicating the temperature-induced change of poled domains is irreversible. Noting that time relaxation may possibly induce back-switching in poled ceramics [39]. We have checked that the poled state maintains for 24 h at room temperature, avoiding the time relaxation influence in this work.

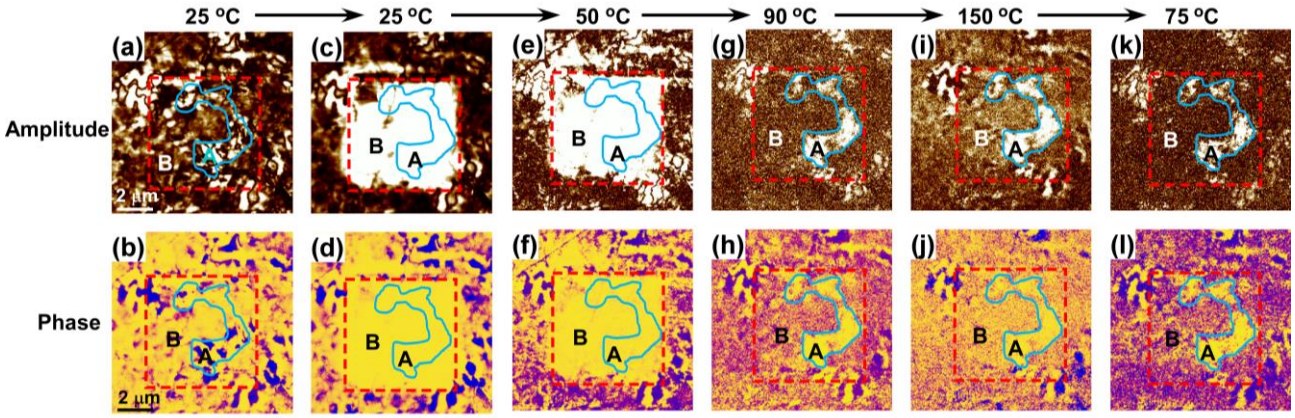

Fig. 5 Temperature-dependent poled domain evolution in a BNT-6BT ceramic. (a) and (b) Out-of-plane amplitude and phase images at 25 ^{o}C before poling. (c) and (d) An inner square in red frame poled by a DC voltage. The corresponding amplitude evolution as a function of temperature:

(e) 50 °C, (g) 90 °C, (i) 150 °C, (k) 75 °C, respectively. The corresponding phase evolution as a function of temperature: (f) 50 °C, (h) 90 °C, (j) 150 °C, (l) 75 °C, respectively.

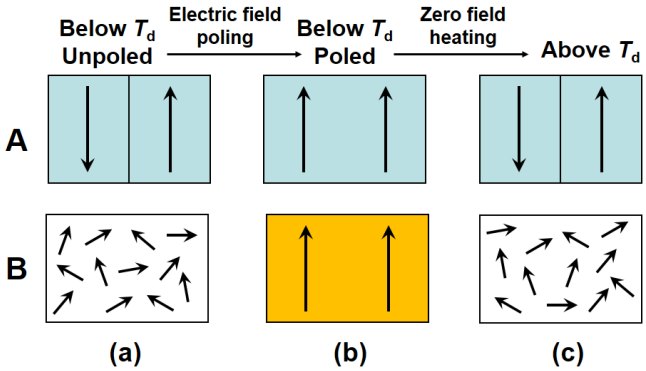

Fig. 6 Schematic of the domain evolution in regard to electric field poling and zero-field heating in region A and region B (as labeled in Fig. 5). (a) Long-range ordered polarization with mesoscopic ferroelectric domains visible by PFM in region A and short-range ordered polarization with domains invisible by PFM in region B. (b) After poling, the long-range ordered ferroelectric domains in both regions A and B. (c) Upon zero field heating above T_d, the long-range ordered ferroelectric domain returns to the polydomain polar state in region A and randomly oriented short-range polarizations in region B.

4. Discussion

The XRD analysis suggests that in BNT-6BT a tetragonal phase and a cubic phase coexist in the average structure, which is in agreement with some literature reports [11]. The domain patterns and domain evolution process observed by PFM are consistent with the Rietveld-refined structural models. There are domains with a strong ferroelectric response embedded in a matrix of blurry phase-contrast, corresponding to the ferroelectric tetragonal phase and an average cubic phase, respectively. Note that in the cubic phase, there might be domains of a size of only a few nanometers

which is below the resolution of PFM if the local structure is non-centrosymmetric. Therefore, these are the domains that may exist but "invisible" to PFM. The frequency dependence of the dielectric permittivity near T_s suggests a relaxor-ferroelectric nature of this material. Therefore, we believe that the relaxor behaviour in this ceramic is related to this average cubic phase based on the following reasons: 1) The regions without long-range ferroelectric domains can be effectively poled, which is characteristic of locally disordered relaxors. Furthermore, upon heating, the temperature-dependent domain contrast in the cubic region A reveals a depoling temperature which is consistent with what is observed in the dielectric permittivity. 2) Near the temperature T_s where the dielectric response exhibits frequency dispersion, no structural change can be detected by X-ray diffraction and no domain pattern change can be observed by PFM in the tetragonal component for an unpoled sample. It was also reported in many BNT-based ceramics and crystals that the dielectric shoulder develops before the dielectric permittivity reaches its maximum, while no phase transition was confirmed around the T_s [33, 34, 37]. This suggests that this dielectric dispersion around T_s is not related to a long-range phase transition in the ferroelectric phase, but rather a relaxor behavior [25].

The domain configurations for the ferroelectric phase and the relaxor phase as well as their evolutions under electric field are schematically shown in Fig. 6. After poling, the BNT-6BT sample exhibits homogeneous out-of-plane projection of the polarizations that is switched to one preferred direction. A careful investigation on different regions on the surface of the sample suggests two transitions happen after poling, *i.e.* the switching of the ferroelectric domains to one preferred direction in region A, and the long-range ordered ferroelectric domain induced from the local polarizations in region B (Fig. 6(b)). The application of an electric field increases the long-range ordering, thereby increasing the ferroelectric interactions over a larger scale, as confirmed by the

XRD and Raman measurements in the literature [2, 27].

The depoling temperature T_d is the highest useful temperature for applications. A T_d of around 76 ^oC is observed in the poled BNT-6BT ceramic, where the piezoelectric response fades away accompanied by a transition from the ferroelectric state to a relaxor state. It is possible that two processes happen around T_d [28]. Firstly, the detexturization of the long-range ordered ferroelectric domains induced by an electric field. Secondly, the transition from the electric field-induced ferroelectric phase to the relaxor state. We have clearly observed these two kinds of transition simultaneously, as shown in Fig. 6(c). The long-range ordered ferroelectric domain induced from the ferroelectric phase returns to the polydomain polar state (ferroelectric phase) above T_d. While, the ordered ferroelectric domain induced from the relaxor phase returns to the "invisible" state (relaxor state) with randomly oriented short-range polarization, suggesting the recovery of the cubic phase component upon heating.

5. Conclusions

The tetragonal and cubic phases are found to coexist in BNT-6BT of the MPB composition. The ferroelectric nanodomains and short-range ordered polarizations "invisible" to PFM resulting from two different structures are observed indirectly. The ferroelectric nanodomains remain stable from room temperature up to 200 ^oC, and no variation is observed going through the T_s. Application of an electric field induces the transition from a relaxor state to a ferroelectric phase and increases the long-range ordering of ferroelectric domains. The ferroelectric nanodomains and "invisible" domains exhibit different behaviors after poling as a function of temperature. Heating breaks the long-range ferroelectric domains and reestablishes the relaxor state above T_d, *i.e.*, rearrangement of polydomain

polar state in the tetragonal phase region and the reappear of “invisible” state in the cubic phase region. The mesoscopic-scale domain structure investigation in the MPB composition is significant for the understanding of the MPB native and its effects on the electric properties of this lead-free system. This systematically combined mesoscopic domains and crystal structure studies provides a better understanding of the structure-property relationship in the BNT-BT solid solution, which in turn will promote the use of lead-free piezoceramics in technological applications.

Acknowledgements

This work was supported by the Natural Science Foundation of China (Grant No. 51332003, 51202184, 91323303, 51602247, 61604123), Natural Science Fundamental research Project of Shaanxi province of China (No. 2017JQ6003), and the “111 Project” of China (B14040). ZG Ye also acknowledgements the supports from the U.S. Office of Naval Research (ONR, Grants No. N00014-12-1-1045 and No. N00014-16-1-3106) and the Natural Sciences and Research Council of Canada (NSERC, Grant No. 203773). JY Zhao would like to thank XJTU and NSERC for supporting her studies at SFU.

References

[1] McQuade RR, Dolgos MR. A review of the structure-property relationships in lead-free piezoelectric (1-*x*)$Na_{0.5}Bi_{0.5}TiO_3$-(*x*)$BaTiO_3$. J. Solid State Chem. 2016;0022:4596.

[2] Maurya D, Pramanick A, Feygenson M, Neuefeind JC, Bodnar RJ, Priya S. Effect of poling on nanodomains and nanoscale structure in A-site disordered lead-free piezoelectric $Na_{0.5}Bi_{0.5}TiO_3$-$BaTiO_3$. J. Mater. Chem. C 2014;2(39):8423-8431.

[3] Yan XW, Ji HF, Lam KH, Chen RM, Zheng F, Ren W, et al. Lead-free BNT composite film for high-frequency broadband ultrasonic transducer applications. IEEE T. Ultrason. Ferr. 2013;60(7):1533-1537.

[4] Ranjan R, Dviwedi A. Structure and dielectric properties of $(Na_{0.50}Bi_{0.50})_{(1-x)}Ba_xTiO_3$: $0 \leq x \leq 0.10$. Solid State Commun. 2005;135(6):394-399.

[5] Rout D, Moon KS, Rao VS, S. Kang JL. Study of the morphotropic phase boundary in the lead-free $Na_{1/2}Bi_{1/2}TiO_3$-$BaTiO_3$ system by raman spectroscopy. J. Ceram. Soc. Jpn. 2009;117(1367):797-800.

[6] Jo W, Daniels JE, Jones JL, Tan XL, Thomas PA, Damjanovic D, et al. Evolving morphotropic phase boundary in lead-free $(Bi_{1/2}Na_{1/2})TiO_3$-$BaTiO_3$ piezoceramics. J. Appl. Phys. 2011;109(1):014110.

[7] Wylie-van Eerd B, Damjanovic D, Klein N, Setter N, Trodahl J. Structural complexity of $(Na_{0.5}Bi_{0.5})TiO_3$-$BaTiO_3$ as revealed by raman spectroscopy. Phys. Rev. B 2010;82(10):104112.

[8] Xu CG, Lin DM, Kwok KW. Structure, electrical properties and depolarization temperature of $(Bi_{0.5}Na_{0.5})TiO_3$-$BaTiO_3$ lead-free piezoelectric ceramics. Solid State Sci. 2008;10(7):934-940.

[9] Takenaka T, Maruyama K, Sakata K. $(Bi_{1/2}Na_{1/2})TiO_3$-$BaTiO_3$ system for lead-free piezoelectric ceramics. Jpn. J. Appl. Phys. Part 1 - Regul. Pap. Short Notes Rev. Pap. 1991;30(9B):2236-2239.

[10] Datta K, Richter A, Gobbels M, Neder RB, Mihailova B. Atomistic origin of huge response functions at the morphotropic phase boundary of $(1-x)Na_{0.5}Bi_{0.5}TiO_3$-$xBaTiO_3$. Phys. Rev. B 2014;90(6):064112.

[11] Garg R, Rao BN, Senyshyn A, Krishna P, Ranjan R. Lead-free piezoelectric system

$(Na_{0.5}Bi_{0.5})TiO_3$-$BaTiO_3$: Equilibrium structures and irreversible structural transformations driven by electric field and mechanical impact. Phys. Rev. B 2013;88(1):014103.

[12] Chen M, Xu Q, Kim BH, Ahn BK, Ko JH, Kang WJ, et al. Structure and electrical properties of $(Na_{0.5}Bi_{0.5})_{(1-x)}Ba_xTiO_3$ piezoelectric ceramics. J. Eur. Ceram. Soc. 2008;28(4):843-849.

[13] Daniels JE, Jo W, Rödel J, Jones JL. Electric-field-induced phase transformation at a lead-free morphotropic phase boundary: Case study in a 93%$(Bi_{0.5}Na_{0.5})TiO_3$-7%$BaTiO_3$ piezoelectric ceramic. Appl. Phys. Lett. 2009;95(3):032904.

[14] Zhang ST, Kounga AB, Aulbach E, Ehrenberg H, Rödel J. Giant strain in lead-free piezoceramics $Bi_{0.5}Na_{0.5}TiO_3$-$BaTiO_3$-$K_{0.5}Na_{0.5}NbO_3$ system. Appl. Phys. Lett. 2007;91(11):112906.

[15] Groszewicz PB, Breitzke H, Dittmer R, Sapper E, Jo W, Buntkowsky G, et al. Nanoscale phase quantification in lead-free $(Bi_{1/2}Na_{1/2})TiO_3$-$BaTiO_3$ relaxor ferroelectrics by means of ^{23}Na NMR. Phys. Rev. B 2014;90(22):220104.

[16] Nagarajan V, Roytburd A, Stanishevsky A, Prasertchoung S, Zhao T, Chen L, et al. Dynamics of ferroelastic domains in ferroelectric thin films. Nat. Mater. 2003;2(1):43-47.

[17] Pramanick A, Prewitt AD, Forrester JS, Jones JL. Domains, domain walls and defects in perovskite ferroelectric oxides: A review of present understanding and recent contributions. Crit. Rev. Solid State 2012;37(4):243-275.

[18] Catalan G, Seidel J, Ramesh R, Scott JF. Domain wall nanoelectronics. Rev. Mod. Phys. 2012;84(1):119-156.

[19] Gobeljic D, Shvartsman VV, Belianinov A, Okatan B, Jesse S, Kalinin SV, et al. Nanoscale mapping of heterogeneity of the polarization reversal in lead-free relaxor-ferroelectric ceramic

composites. Nanoscale 2016;8(4):2168-2176.

[20] Zhao JY, Ren W, Niu G, Zhang N, Dong GH, Wang LY, et al. Recoverable self-polarization in lead-free bismuth sodium titanate piezoelectric thin films. ACS Appl. Mater. Interfaces 2017;9(34):28716-28725.

[21] Maurya D, Pramanick A, An K, Priya S. Enhanced piezoelectricity and nature of electric-field induced structural phase transformation in textured lead-free piezoelectric $Na_{0.5}Bi_{0.5}TiO_3$-$BaTiO_3$ ceramics. Appl. Phys. Lett. 2012;100(17):172906.

[22] Viola G, Ning HP, Wei XJ, Deluca M, Adomkevicius A, Khaliq J, et al. Dielectric relaxation, lattice dynamics and polarization mechanisms in $Bi_{0.5}Na_{0.5}TiO_3$-based lead-free ceramics. J. Appl. Phys. 2013;114(1):014107.

[23] Groszewicz PB, Gröting M, Breitzke H, Jo W, Albe K, Buntkowsky G, et al. Reconciling local structure disorder and the relaxor state in $(Bi_{1/2}Na_{1/2})TiO_3$-$BaTiO_3$. Sci. Rep. 2016;6:31739.

[24] Schader FH, Wang ZY, Hinterstein M, Daniels JE, Webber KG. Stress-modulated relaxor-to-ferroelectric transition in lead-free $(Na_{1/2}Bi_{1/2})TiO_3$-$BaTiO_3$ ferroelectrics. Phys. Rev. B 2016;93(13):134111.

[25] Bokov AA, Ye ZG. Recent progress in relaxor ferroelectrics with perovskite structure. J. Mater. Sci. 2006;41(1):31-52.

[26] Sapper E, Dittmer R, Damjanovic D, Erdem E, Keeble DJ, Jo W, et al. Aging in the relaxor and ferroelectric state of Fe-doped $(1-x)(Bi_{1/2}Na_{1/2})TiO_3$-$xBaTiO_3$ piezoelectric ceramics. J. Appl. Phys. 2014;116(10):104102.

[27] Craciun F, Galassi C, Birjega R. Electric-field-induced and spontaneous relaxor-ferroelectric phase transitions in $(Na_{1/2}Bi_{1/2})_{(1-x)}Ba_xTiO_3$. J. Appl. Phys. 2012;112(12):124106.

[28] Jo W, Daniels J, Damjanovic D, Kleemann W, Rödel J. Two-stage processes of electrically induced-ferroelectric to relaxor transition in 0.94($Bi_{1/2}Na_{1/2}$)TiO_3-0.06$BaTiO_3$. Appl. Phys. Lett. 2013;102(19):192903.

[29] Lidjici H, Lagoun B, Berrahal M, Rguitti M, Hentatti MA, Khemakhem H. XRD, raman and electrical studies on the (1-*x*)($Na_{0.5}Bi_{0.5}$)TiO_3-*x*$BaTiO_3$ lead free ceramics. J. Alloy. Compd. 2015;618:643-648.

[30] Maurya D, Petkov V, Kumar A, Priya S. Nanostructured lead-free ferroelectric $Na_{0.5}Bi_{0.5}TiO_3$-$BaTiO_3$ whiskers: synthesis mechanism and structure. Dalton T 2012;41(18):5643-5652.

[31] Ma C, Tan X, Dul'kin E, Roth M. Domain structure-dielectric property relationship in lead-free (1-*x*)($Bi_{1/2}Na_{1/2}$)TiO_3-*x*$BaTiO_3$ ceramics. J. Appl. Phys. 2010;108(10):104105.

[32] Stephens PW. Phenomenological model of anisotropic peak broadening in powder diffraction. J. Appl. Crystallogr 1999;32:281-289.

[33] Vakhrushev SB, Isupov VA, Kvyatkovsky BE, Okuneva NM, Pronin IP, Smolensky GA, et al. Syrnikov. Phase-transitions and soft modes in sodium bismuth titanate. Ferroelectrics 1985;63(1-4):153-160.

[34] Zhang MS, Scott JF, Zvirgzds JA. Raman-spectroscopy of $Na_{0.5}Bi_{0.5}TiO_3$. Ferroelectr. Lett. Sect. 1986;6(5):147-152.

[35] Jones GO, Thomas PA. Investigation of the structure and phase transitions in the novel A-site substituted distorted perovskite compound $Na_{0.5}Bi_{0.5}TiO_3$. Acta Crystallogr. Sect. B-Struct. Sci. 2002;8:168-178.

[36] Pronin IP, Syrnikov PP, Isupov VA, Egorov VM, Zaitseva NV. Peculiarities of phase-transitions

in sodium-bismuth titanate. Ferroelectrics 1980;25(1-4):395-397.

[37] Yao JJ, Ge WW, Luo L, Li JF, Viehland D, Luo HS. Hierarchical domains in $Na_{1/2}Bi_{1/2}TiO_3$ single crystals: Ferroelectric phase transformations within the geometrical restrictions of a ferroelastic inheritance. Appl. Phys. Lett. 2010;96(22):222905.

[38] Jo W, Schaab S, Sapper E, Schmitt LA, Kleebe H, Bell AJ, et al. On the phase identity and its thermal evolution of lead free $(Bi_{1/2}Na_{1/2})TiO_3$-6mol% $BaTiO_3$. J. Appl. Phys. 2011;110(7):074106.

[39] Dittmer R, Jo W, Rödel J, Kalinin S, Balke N. Nanoscale insight into lead-free BNT-BT-*x*KNN. Adv. Funct. Mater. 2012;22(20):4208-4215.

Graphic abstrate

The mesoscopic domain structure and behavior of BNT-BT, in relation to the macroscopic crystal structure and dielectric permittivity, are studied systematically to give an insight into its long-, medium- and short-range ordering. The ferroelectric nanodomains and possibly local polarizations “invisible” to PFM coexisting in the ceramic samples are related to a tetragonal (ferroelectric state) and a cubic (relaxor state) phase, and exhibit different behaviors with electric field or temperature change.